ESTIMATING RICE PLANT COVERAGE IN PADDY FIELDS USING UAV AND SENTINEL-2

Yuki Sato[1] , Masayuki Matsuoka[*2] and Takeshi Tsuji[3]
[1]Graduate Student, Department of Information Engineering, Mie University,
1557, Kurima Machiya-cho, Tsu City, Mie Prefecture 514-8507
Email: 422m518@m.mie-u.ac.jp

[2]Associate Professor, Department of Information Engineering, Mie University,
1557 Kurima Machiya-cho, Tsu City, Mie Prefecture 514-8507
Email: matsuoka@info.mie-u.ac.jp

[3]Tsuji Farm Co.
1211 Osato Mutsuai-cho, Tsu City, Mie Prefecture 514-0126
Email: ttake@tarafuku.org

KEY WORDS: Unmanned Aerial Vehicle (UAV), Sentinel-2, Paddy field, Rice plant coverage, Mixed pixel analysis

ABSTRACT: Satellite remote sensing is used to determine the spatial distribution of crop growth in large agricultural areas. Due to the low resolution of satellites, it is difficult to accurately monitor the growth of paddy rice. For this reason, monitoring using unmanned aerial vehicles (UAVs), which have higher resolution, is often used to determine the growth conditions more accurately. The objective of this study is to calculate rice plant coverage from satellite images. We applied the spectral unmixing method to calculate the rice plant coverage from UAV images. After that, we saw if there was a correlation with the observed values from satellite images on a pixel-by-pixel basis. The field measurement was conducted in rice paddies in Tsu City, Mie Prefecture.

1. INTRODUCTION

1.1 Motivation

In recent years, the number of farmers in the Japanese agricultural industry has been declining and the amount of abandoned farmland has been increasing. In order to solve these problems, the local government has been promoting the concentration and agglomeration of farmlands. The concentration of farmlands accelerated in 2014 with the establishment of the Agricultural Land Bank. As a result, the concentration rate in FY2021 was 58.9%. In addition, the number of new agricultural corporations has been steadily increasing (Ministry of Agriculture, Forestry and Fisheries, 2022, 2023). As these trends indicate, there is a need to improve the efficiency of the agricultural industry.

"Smart agriculture" which utilizes advanced technologies such as robots, AI, and IoT, is expected to dramatically improve productivity through work automation and data sensing technology. Many studies have been conducted in the agricultural field on remote sensing using satellites and aircraft. Meanwhile, remote sensing using Unmanned Aerial Vehicles (UAV) has been attracting attention in recent years. UAVs are expected to be used for detailed observation of the field because they have high spatial resolution and flexible observation capabilities (Inoue, 2023).

1.2 Aims

The study aims to estimate rice plant coverage from satellite images with high accuracy. It is difficult to monitor crop conditions because of the low resolution of the satellites in comparison to UAVs. Therefore, we studied in the order of the following steps using Sentinel-2 and UAV images.

Step 1. Registration of UAV and Sentinel-2 reflectance images.
Step 2. Calculation of UAV rice coverage images with the spectral unmixing method.
Step 3. Generation of a model for estimating Sentinel-2 rice coverage images with multiple regression analysis.

1.3 Related work

Various studies have suggested that UAVs can be used to estimate rice coverage and yield. Yoshimura et al. (2016) calculated the green coverage of dent corn during the growing season using maximum likelihood classification. Zheng et al. (2020) proposed a new decision tree model that combines texture features and spectral features to detect rice plants in

UAV images. Yuan et al. (2021) found that adaptive spectral endmembers and a bilinear mixing model improved yield estimation accuracy in rice crops. Wan et al. (2020) found that fusing spectral and structural information extracted from UAV images improved grain yield prediction accuracy.

The mixed pixel analysis used in this study has been investigated by several researchers. Fujita et al. (2013) combined MODIS NDVI and Landsat TM images and obtained endmember NDVI seasonal changes using the spectral unmixing method. As a result, it was shown that NDVI seasonal changes for each crop could be estimated with high accuracy. In addition, the determination of endmembers is important in conducting the mixed pixel analysis. Some methods include referring to spectral information of endmembers observed and collected in the field or laboratory or extracting them from images. Oki et al. (2002) used spectral information measured in the laboratory to estimate the vegetation coverage with different levels of activity by the unmixed spectral method. Awadu et al. (2003) propose a method to estimate the endmembers of crops and soils in a pixel and their coverage in a situation where the endmembers are unknown.

In this study, the reflectance showed a large variation due to the difference in solar radiation at the time of observation. Several studies have considered these solar radiation conditions. Hashimoto et al. (2020) proposed a new LAI estimation method by machine learning with solar radiation conditions added as a variable. Ono et al. (2002) showed that topographic and atmospheric effects can be suppressed by normalizing the reflectance obtained from satellites using the mean value of the bands. Ono et al. (2013) normalized green, red, and near-infrared reflectance data from the Advanced Visible and Near Infrared Radiometer Type-Ⅱ (AVNIR-2) with an additive average of three bands. The results showed that the data were less affected by sunlight and weather conditions.

2. DATA ACQUISITION

2.1 Study Area

The field measurements were conducted at Tsuji Farm, located in Tsu City, Mie Prefecture (136°29’E, 34°46’N) (Figure 1). This field is divided into 13 plots. Among them, five plots (A, C, D, E, F, and G) are used in this study, and the rice species is "Mie no Yume". The rice was planted on June 16 and 17, 2023.

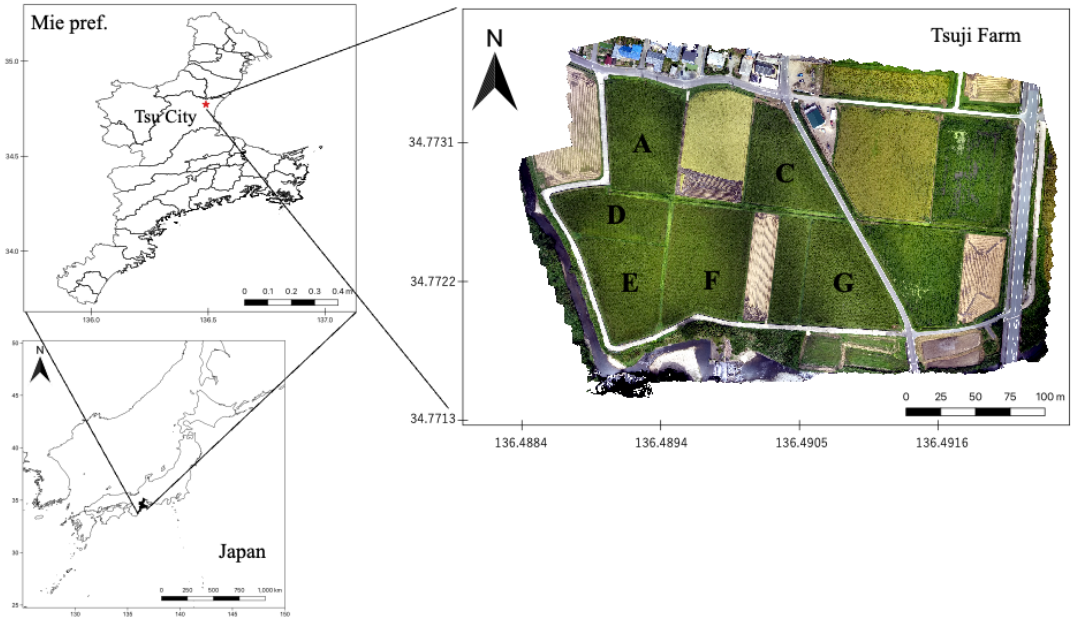

Figure 1. Study area in Tsuji Farm, Tsu City, Mie Prefecture. Symbols A, C to G represent the research plots.

2.2 UAV and Sentinel-2

The UAV used in this study was a P4 Multispectral (DJI Inc.), which is equipped with a 5-band (blue, green, red, red-edge, and near-infrared) multispectral camera. The camera specifications are shown in Table 1. We used the software DJI GS Pro (DJI Inc.) for automatic measurements at 60 m altitude. We also set the camera to equal time interval shooting mode with 70% overlap and 90% sidelap. The observations were conducted under sunny or cloudy conditions with low wind speeds.

Table1. Technical specifications of UAV multispectral camera

Aircraft		DJI PHANTOM 4 Pro
Camera		DJI P4 Multispectral
Dimension (cm)		35 (diagonal size)
Take-off weight (g)		1487
Spectral range of the band (nm)	blue	456 ± 16
	green	560 ± 16
	red	650 ± 16
	red Edge	730 ± 16
	NIR	840 ± 26
Sensor resolution (mega pixel)		2.08
Image size (pixel)		1600 × 1300
GSD on 60 m flight altitude (cm)		approximately 3.2
Field of view (°)		62.7

Satellite images were bands 2, 3, 4, and 8 of Multispectral Instrument (MSI) onboard Sentinel-2. The product type is the level 1C. The MSI was used for satellite images because they have higher spatial (10 m) and temporal (5 days) resolutions than other mid-spatial resolution images. The data were downloaded via Copernicus Open Access Hub, considering the geographic locations, season, and cloud coverage.

The UAV images used in the study were acquired in six days between June 16 and September 2, with June 16 measured just prior to planting. We selected the cloud-free Sentinel-2 image closest date to the UAV observation. The image corresponding to September 2 could not be acquired due to bad weather conditions (Table 2).

Table 2. Observation dates of UAV and Sentinel-2/MSI data

UAV	Sentinel-2
2023-06-16T10:40:00	2023-06-19T10:37:01
2023-06-29T10:40:00	2023-07-04T10:36:59
2023-07-14T10:35:00	2023-07-24T10:36:59
2023-07-27T10:35:00	2023-07-29T10:37:01
2023-08-17T10:50:00	2023-08-13T10:36:59
2023-09-02T11:20:00	-

3. METHOD

The major flow of this study is shown in Figure 2.

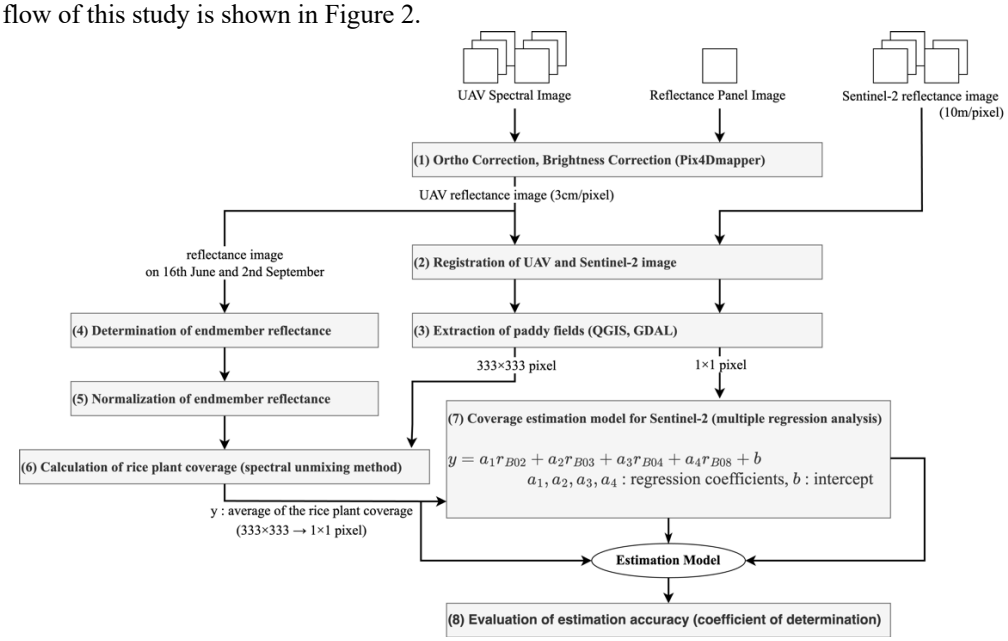

Figure 2. Flowchart of image analysis

3.1 Generation of Reflectance Images

Orthorectified reflectance images were created using Pix4Dmapper (Pix4D). The spatial resolution of this image was 0.03 m. Radiometric correction was performed with a calibrated reflectance panel.

3.2 Registration of UAV and Sentinel-2 Images

The UAV image was shifted to improve the geometric registration accuracy between the UAV and the Sentinel-2 images. Since UAV images have much higher resolution than Sentinel-2 images, we searched the image position with the highest correlation coefficient of images by shifting the UAV images over Sentinel-2 images. The target area was 330 m × 160 m, and the range of grid search was ±9 m with 0.6 m steps both in north-south and west-east directions.

3.3 Extraction of Paddy Fields

Paddy field pixels used in the analysis were extracted from the position-corrected UAV images using QGIS. The process was conducted as follows: (1) 10 m × 10 m polygons were set at the center of the paddy field to match the resolution of the satellite. (2) the UAV and Sentinel-2 images were cropped corresponding to the above polygons. NIR band images of the UAV and Sentinel-2 with the polygons are shown in Figure 3.

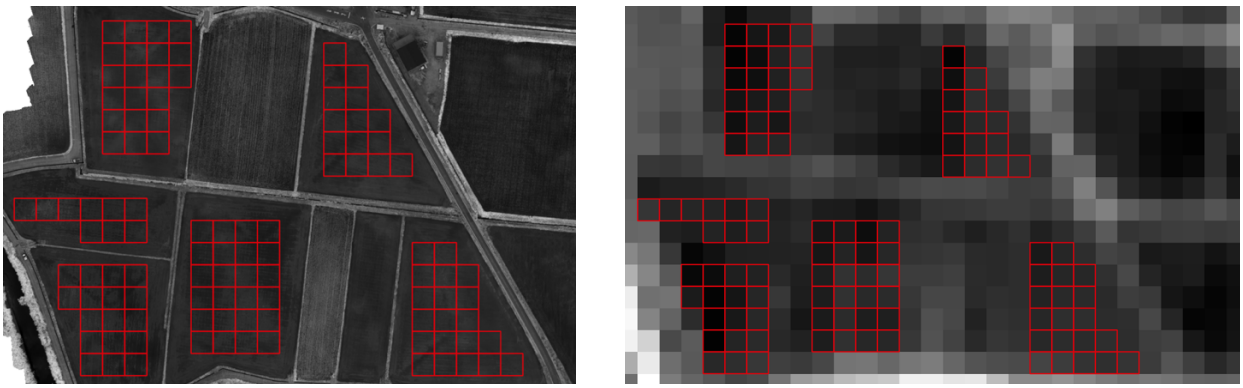

(a) UAV image on 16th June 2023 (b) Sentinel-2 image on 19th June 2023

Figure 3. Extraction of paddy field pixels

3.4 The Spectral Unmixing Method

Most land cover classification methods in remote sensing assume that a pixel consists of a single land cover element. However, a pixel often contains more than one category. Such pixels are called “mixed pixels”, and this problem usually occurs in low-resolution images. The spectral unmixing method solves this problem.

Mixed pixels contain multiple properties and exhibit different properties from pure pixels. Therefore, the reflectance of an observed pixel can be assumed to be a linear combination of the reflectance and the areal fraction of its components (Equation (1)). The components are called endmembers, which are substances such as vegetation, soil, and water contained within the pixel. In other words, the spectral unmixing method can be used to estimate the endmember areal fraction from the endmember and observed reflectance. The observed reflectance is expressed as follows:

$$y_i = \sum_{k=1}^{M} a_k x_{ik} \qquad (1),$$

where y_i: reflectance of the pixel at band i, M: the number of endmembers, x_{ik}: known reflectance of endmember k in band i, a_k: unknown areal fraction of endmember k.

3.5 Reflectance of Endmembers

Since the target site is a paddy field, the endmembers are rice and water. In this study, the endmember's reflectance was extracted from UAV multispectral images. Therefore, M = 2 (water and rice), and i is five (blue, green, red, red-edge, NIR) in Equation (1). Specifically, the reflectance was extracted from randomly selected 500 pixels in plot A observed on 16th June and 2nd September for water and rice. As a reason for that, rice was not planted on 16th June and covered

about 100% on 2nd September. The average of the values was then used for the endmember's reflectance. In addition, the respective reflectance was normalized by the additive mean reflectance of all bands in order to suppress differences in observation conditions (Equation (2), (3)). In other words, the observed reflectance of the mixed pixel can be expressed in Equation (4) in this study.

$$\boldsymbol{r_0 = r_{blue} + r_{green} + r_{red} + r_{rededge} + r_{NIR}} \quad (2),$$

$$\boldsymbol{NR_{blue} = \frac{r_{blue}}{r_0}, NR_{green}r = \frac{r_{green}}{r_0}, \dots, NR_{NIR} = \frac{r_{NIR}}{r_0}} \quad (3),$$

$$\boldsymbol{P = \rho_w NR_w + \rho_r NR_r} \quad (4),$$

where P: measured reflectance of the mixed pixel, ρ_w, ρ_r: areal fraction of water and rice, NR_w, NR_r: normalized reflectance of water and rice.

3.6 The Constrained Least Squares Method

The main approaches to the spectral unmixing methods are (1) constrained least squares, (2) fuzzy membership methods, (3) methods based on geometric models, and (4) methods based on establishment models (Kitamoto, 2003). In this study, the areal fraction is calculated by the least-squares method under the conditions $\rho_w + \rho_r = 1,\ \rho_w, \rho_r > 0$ (ρ_w, ρ_r is the areal fraction of water and rice).

The areal fraction of rice and water was calculated by substituting all rice paddy pixels in the UAV reflectance image into P in Equation (4) and solving for it using the conditional least squares method. ρ_r was used as the pixel value to create a rice coverage map.

3.7 Relationship between Sentinel-2 Reflectance and Rice Plant Coverage

We calculate the relationship between rice plant coverage and Sentinel-2 reflectance in order to estimate rice plant coverage from the Sentinel-2 images. The average of the coverage map for each polygon is compared to the corresponding Sentinel-2 reflectance. We conducted multiple regression analyses with Sentinel-2 bands as the independent variable and the rice plant coverage as the dependent variable. We used the coefficient of determination (R-squared) for the evaluation, calculated from all data used for the regression.

4. RESULTS AND DISCUSSION

4.1 Evaluation of the Registration Process

We used green and NIR reflectance images to evaluate the registration accuracy because they showed a clear trend in correlation coefficients. Then, we adopted the registration with the higher correlation coefficient of the two band images. As a trend, the correlation coefficient was higher in the NIR band when the rice plants were small. On the other hand, it was higher for the green band when the rice plants were in the growing stage. This is due to the large proportion of paddy fields occupying the registration target area, which affected the reflectance as the rice grows. Figure 4 (a) shows a scatter diagram of the UAV and Sentinel-2 NIR reflectances with and without precise registration on June 19th. When superimposed without any processing, the correlation coefficient is 0.82. On the other hand, the correlation coefficient is 0.91 after registration processing. This result shows the effectiveness of the registration process. Figure 4 (b) shows a scatter diagram of the UAV and Sentinel-2 green band's reflectances with and without precise registration on July 29th.

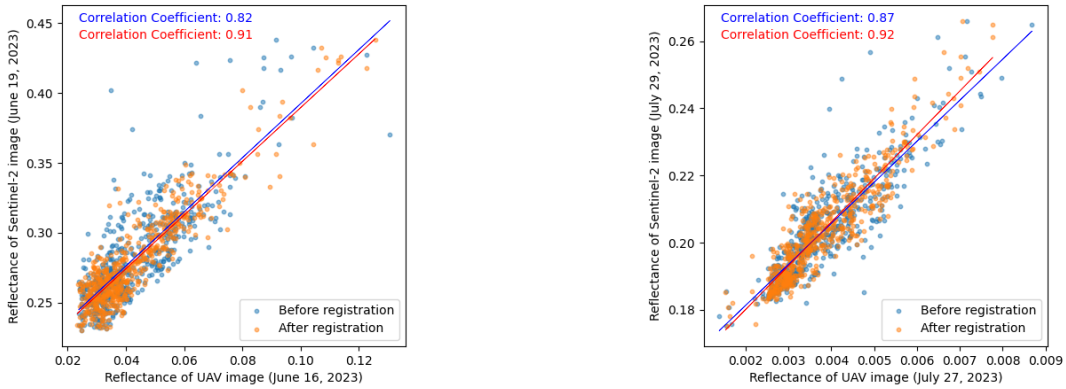

(a) Immediately after planting (band: NIR) (b) growing season (band: Green)

Figure 4. Comparison of reflectance between before and after registration.

4.2 Evaluation of the spectral Unmixing Method

The changes in rice coverage in plot A are shown in Figure 5. For each day, a spatial distribution of coverage could be shown. In addition, the growth of the rice plants can be seen in detail as time goes. While there was some variation in coverage by location until July 27, there was almost no variation by August 17, showing that the coverage was close to 100% for the entire plot.

In addition, the change in the average rice plant coverage for each day is shown in Figure 6. The speed of rice growth from the planting date could be shown. Figure 6 shows that rice plants grow rapidly from 13 to 28 days after planting. After 62 days, the growth rate remained flat. Plot C has a lower coverage than the others, but this is also evident in the RGB orthophoto.

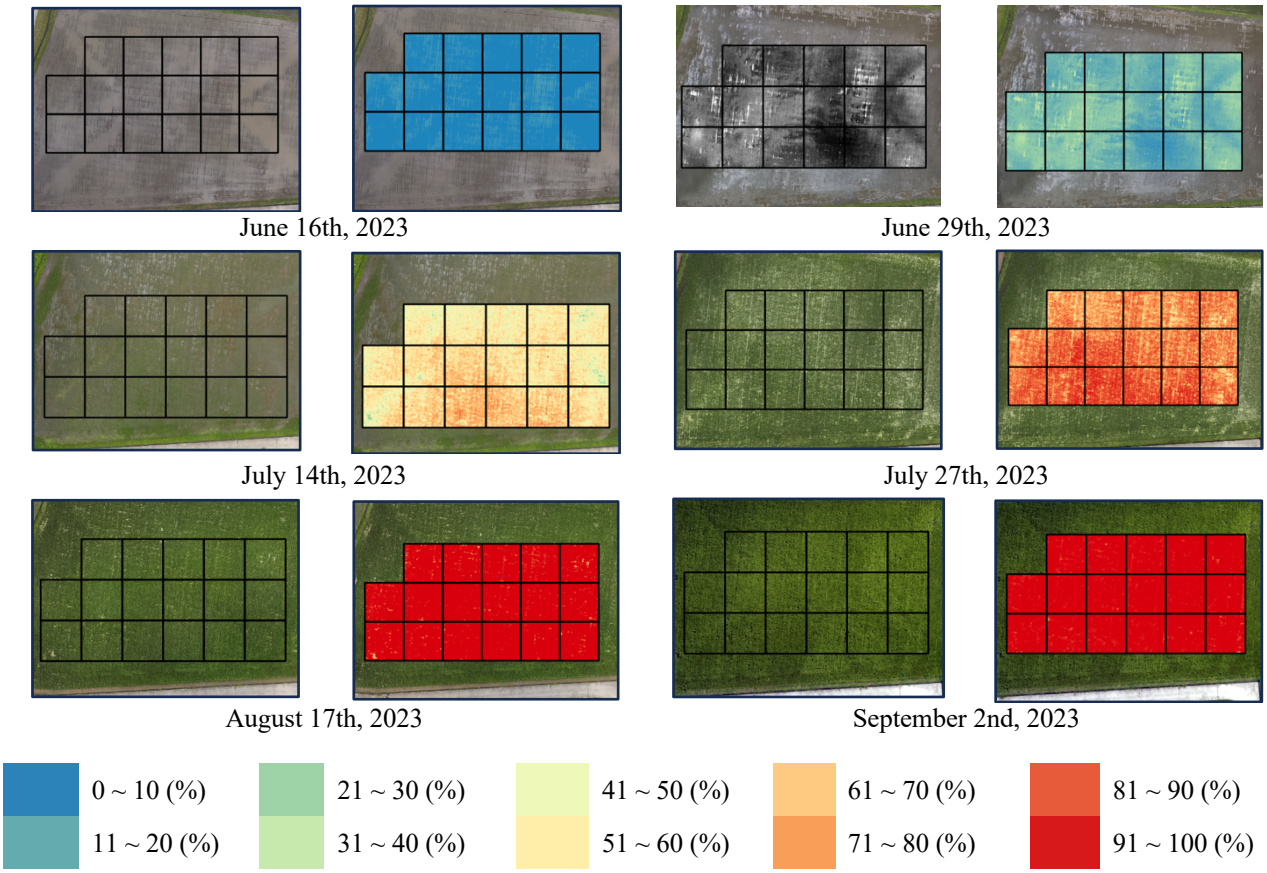

Figure 5. Rice plant coverage map of UAV images (Left: RGB image, Right: coverage map)

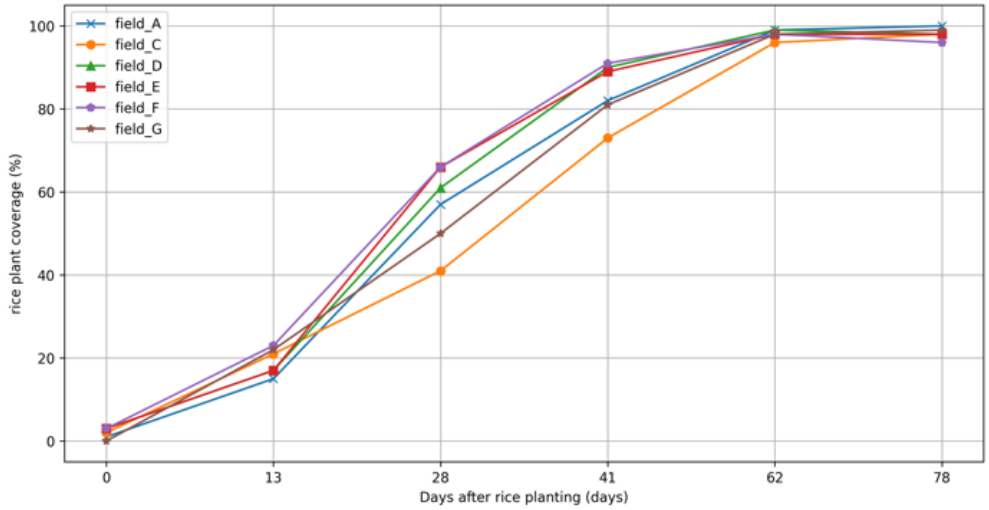

Figure 6. Changes in the average rice plant coverage

4.3 Estimation of the Rice Plant Coverage by Sentinel-2

Figure 7 shows the correlation between the coverage estimates from multiple regression analysis and the coverage calculated by the unmixed spectral method. The regression coefficients were -274.30, -712.32, 261.53, and 393.15 for bands 2, 3, 4, and 8, respectively. The intercept was 77.07. The coefficient of determination was 0.92. Although there are errors, a relatively high estimation accuracy was achieved. We were able to show the potential of the estimation model using Sentinel-2 reflectance images.

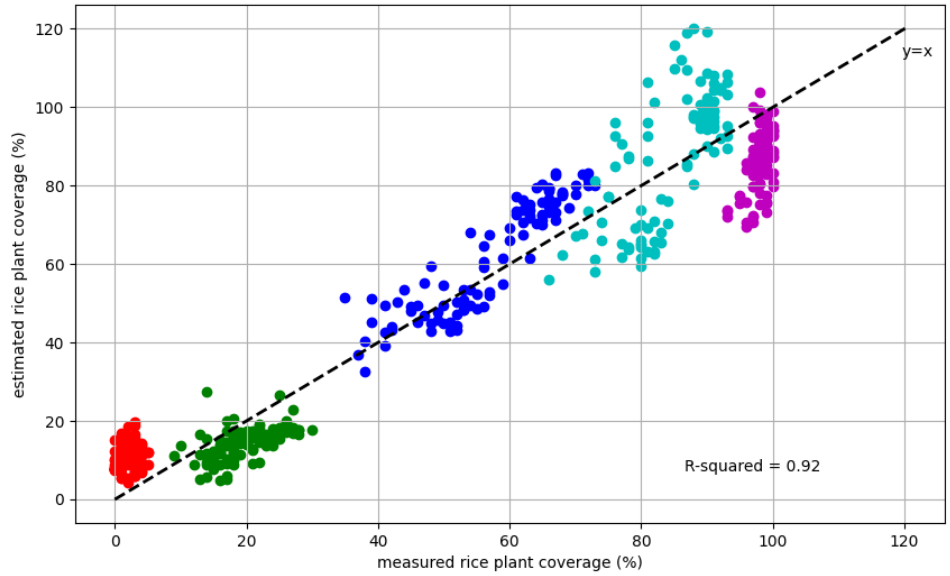

Figure 7. Scatter plots of measured and estimated values

Figure 8 shows the coverage map when the estimated model is applied to all pixels. The spatial coverage can be seen across the entire field. We can see the variation of coverage within a field and the differences between fields. However, as shown in Figure 9, the coverage on July 29 and August 13 is reversed in some locations.

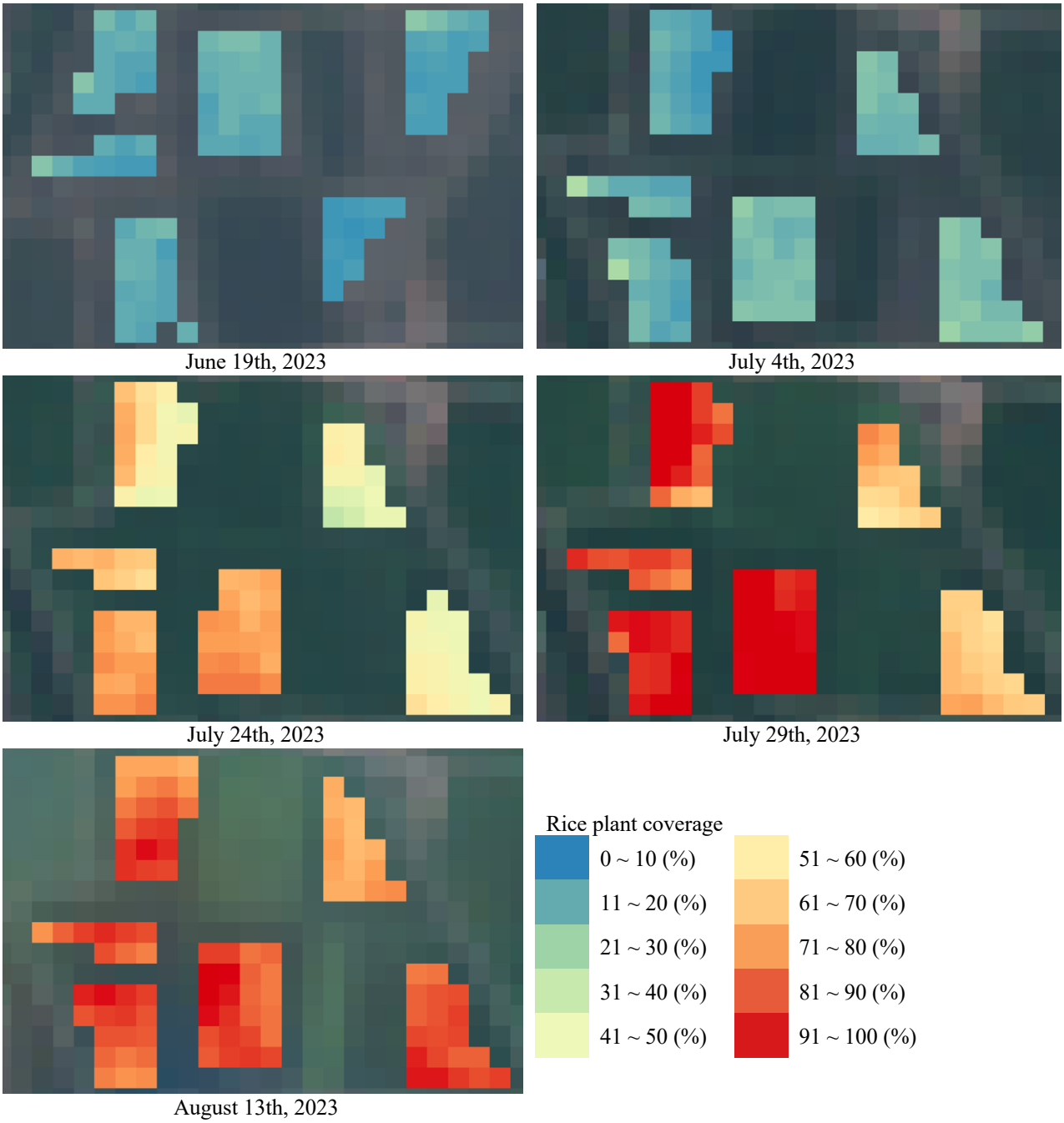

Figure 8. Estimated rice plant coverage map of Sentinel-2 image

In addition, the change in the average estimated rice plant coverage for each day is shown in Figure 9. The speed of rice growth from the planting date could be shown. In all plots, the rice coverage was estimated lower than that calculated by the UAV. Plot C did not reach 80 percent coverage even at 59 days after rice planting. Coverage was estimated to be higher at 43 days after rice planting than at 59 days. This is because of the Sentinel-2 image on August 13 (59 days after rice planting) is covered by thin clouds.

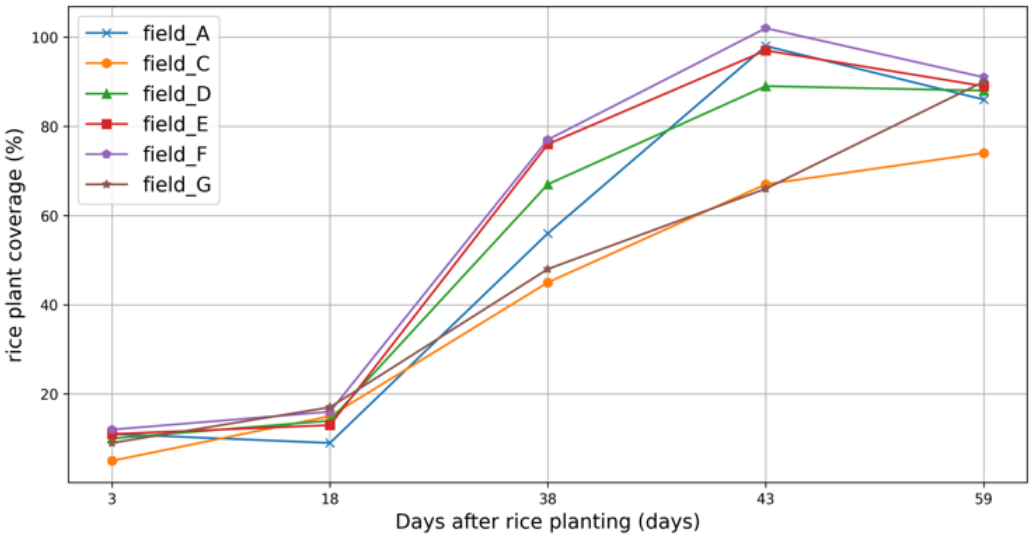

Figure 9. Changes in the average estimated rice plant coverage

5. CONCLUSION

This study used UAV images to determine the rice plant coverage during their growth. We were able to show that the use of the spectral unmixing method in UAV images can provide more detailed information on the condition of rice plants than ever before. In addition, the use of normalized reflectance was able to suppress the differences in sunlight conditions at the time of the image capture. Multiple regression analysis using Sentinel-2 reflectance images also showed high estimation accuracy. However, there are issues that make it unreliable due to differences in the date of the Sentinel-2 and UAV images, clouds prevented the use of Sentinel-2 imagery at certain times of the year. Higher resolution and higher periodicity satellites are now available, and if combined with these newer technologies, a more stable analysis can be performed.

As written in the introduction, we hope that the use of remote sensing technology using UAVs will be promoted in the agricultural sector, where efficient agricultural production is required.

REFERENCES

Awadu, T., Oki, K., Omasa, K., 2003. Endmember Estimation of Mixed Pixel Data in Agricultural Area. *Journal of the Remote Sensing Society of Japan*, 23(5), pp. 543-549. https://doi.org/10.11440/rssj1981.23.543

Da-Jiang Innovations Science and Technology Co., Ltd., P4 Multispectral. https://www.dji.com/p4-multispectral

Fujita, A., Kotera, A., Satir. O., Berberoglu. S., Nagano, T., 2013. Estimation of Pure NDVI Seasonal Profiles of Crops by Temporal Unmixing of MODIS Dataset. *The Japanese Society of Irrigation, Drainage and Rural Engineering*, 81(5), pp. 385-393, https://doi.org/10.11408/jsidre.81.385

Hashimoto, N., Saito, Y., Yamamoto, S., Maki, M., & Homma, K. 2020. Evaluation of Machine Learning to Estimate LAI Including Solar Radiation Condition at UAV Monitoring in Paddy Fields. *Journal of the Remote Sensing Society of Japan*, 40(2), pp. 87-96, https://doi.org/10.11440/rssj.40.87

Inoue, Y., 2023. Utility and Caveats of Sensing and Data Science for Smartification of Crop Production –Remote Sensing, AI, Big Data, and Phenotyping–. *The Crop Science Society of Japan*, 92(2), 91-103, https://doi.org/10.1626/jcs.92.91

Kitamoto, A., Takagi, M., 1996. Mixture Density Estimation In the Presence of Mixels. *IEICE Transactions on Information and Systems*, PRU95-202, pp. 33-40

Ministry of Agriculture, Forestry and Fisheries., 2022. Changes in the Situation Concerning Food, Agriculture, and Rural Areas (Securing bearers in a declining population). https://www.maff.go.jp/j/study/attach/pdf/nouti_housei-1.pdf, (In Japanese)

Ministry of Agriculture, Forestry and Fisheries., 2023. Current Situation and Measures for Dilapidated Farmland. https://www.maff.go.jp/j/nousin/tikei/houkiti/attach/pdf/index-16.pdf, (In Japanese)

Oki, K., Omasa, K., Inamura, M., 2002. Separation of Vegetation Coverage and Vigor for Vegetation Remote Sensing by Unmixing Method –Evaluation of Unmixing Method in Laboratory Experiment–. *Agricultural Meteorology of Japan*. 58(1), 33-39, https://doi.org/10.2480/agrmet.58.33

Ono, A., Fujiwara, N., Ono, A., 2002. Suppression of Topographic and Atmospheric Effects by Normalizing the Radiation Spectrum of Landsat/TM by the Sum of Each Band. *Journal of the Remote Sensing Society of Japan*, 22(3), pp. 318-327, https://doi.org/10.11440/rssj1981.22.318

Ono, A., Ono, A., 2013. Vegetation Analysis of Larix kaempferi Using Radiant Spectra Normalized by Their Arithmetic Mean. *Journal of the Remote Sensing Society of Japan*, 33(3), pp.200-207, https://doi.org/10.11440/rssj.33.200

The European Space Agency, SENTINEL-2 MSI Technical Guide.
https://sentinels.copernicus.eu/web/sentinel/technical-guides/sentinel-2-msi,

Wan, L., Cen, H., Zhu, J., Zhang, J., Zhu, Y., Sun, D., Du, X., Zhai, L., W, H., Li, Y., Li, X., Bao, Y., Shou, J., He, Y., 2020. Grain yield prediction of rice using multi-temporal UAV-based RGB and multispectral images and model transfer - a case study of small farmlands in the South of China. *Agricultural and Forest Meteorology*, Volume 291, https://doi.org/10.1016/j.agrformet.2020.108096

Yoshimura, N., Furukawa, F., Watanabe, Y., Song, L., Ohara, Y., Ogawa, K., Yoshihira, T., 2016. Case Study of High-temporal Monitoring of green Coverage in a Dent Corn Using a Drone. *The Japanese Society of Irrigation, Drainage and Rural Engineering*. 84(9), pp. 773-776, https://doi.org/10.11408/jjsidre.84.9_773

Yuan, N., Gong, Y., Fang, S., Liu, Y. Duan, B., Yang, K., Wu, X., Zhu, R., 2021. UAV Remote Sensing Estimation of Rice Yield Based on Adaptive Spectral Endmembers and Bilinear Mixing Model. *Remote Sensing*, 13, 2190, https://doi.org/ 10.3390/rs13112190

Zheng, H., Zhou, H., He, J., Yao, X., Cheng, T., Zhu, Y., Cao, W., Tian, Y., 2020. Early season detection of rice plants using RGB, NIR-G-B and multispectral images from unmanned aerial vehicle (UAV). *Computers and Electronics in Agriculture*, 169, 105223, https://doi.org/10.1016/j.compag.2020.105223